Lattice-gas-model approach to understanding the structures of lithium transition-metal oxides $LiMO_2$

W. Li, J. N. Reimers, and J. R. Dahn
Department of Physics, Simon Fraser University, Burnaby, British Columbia, Canada V5A 1S6
(Received 19 February 1993; revised manuscript received 27 July 1993)

Many lithium transition-metal oxides ($LiMO_2$, M = Ti, V, Cr, Mn, Fe, Co, Ni) have structures made up of oxygen atoms occupying a cubic close-packed fcc or distorted fcc lattice, with cations occupying all octahedral interstices. The cation lattice is therefore also fcc and the arrangements of the cations on that lattice can be studied with a lattice-gas model. The $LiNiO_2$, layered $LiCoO_2$, spinel $LiCoO_2$, $Li_2Ti_2O_4$, and γ-$LiFeO_2$ structures are predicted for appropriate values of first- (J_1) and second- (J_2) neighbor interactions within such a model by analogy with binary-alloy materials having similar structures. We are able to assign allowable ranges for the interactions for each of the oxides above based on their position in the J_1-J_2-T phase diagram. A surprising result is that the layered and spinel $LiCoO_2$ structures are equally stable over the same wide range of J_1 and J_2, as predicted by mean-field and Monte Carlo results. Although $LiMnO_2$ is structurally related to the above materials, the $LiMnO_2$ structure is not stable for any choice of J_1, J_2, or T. Further neighbor interactions or anisotropies in the near-neighbor interactions are needed to stabilize the $LiMnO_2$ structure.

I. INTRODUCTION

Many lithium transition-metal oxides ($LiMO_2$) (where M is a $3d$ transition metal) have structures derived from cubic close-packed oxygen atoms with cations filling all octahedral interstices. The cation lattice is also fcc and the arrangement of the cations on the lattice determines the structure of the material. The oxygen lattice simply provides a framework of sites in which the cations reside; a perfect scenario for the application of a lattice-gas model. $LiMO_2$ compounds are used in advanced batteries[1,2] and in electrochromic displays.[3] Many of them are intercalation compounds.[4] Therefore, these materials are important to understand for scientific and technical reasons. Here we apply a lattice-gas model to $LiMO_2$ compounds to understand their structures.

Hewston and Chamberland reviewed[5] the structure and properties of $LiMO_2$ compounds. Of these materials $LiNiO_2$, $LiCoO_2$, $LiCrO_2$, $LiVO_2$, $LiTiO_2$, $LiMnO_2$, and γ-$LiFeO_2$ have all been shown to have the Li and M atoms arranged in a superstructure. $LiNiO_2$ (and $LiCrO_2$) have Li and Ni (Cr) atoms segregated into layers normal to one of the cubic $\langle 111 \rangle$ directions. $LiCoO_2$ adopts two structures, the first of which is isostructural to $LiNiO_2$. The second structure, prepared at low temperatures (called LT-$LiCoO_2$), is spinel related[6,7] with cations in the $16c$ (Li) and $16d$ (Co) sites of the space group $Fd\bar{3}m$. $LiVO_2$ also adopts both the layered and spinel structures. $LiTiO_2$, synthesized at high temperature, has disordered cations. However, if it is made by intercalating Li into $LiTi_2O_4$ to make $Li_2Ti_2O_4$, it takes the spinel structure of LT-$LiCoO_2$. The cations in γ-$LiFeO_2$ adopt yet another superlattice ordering which leads to a tetragonal unit cell.[5] $LiMnO_2$ adopts a fourth superlattice arrangement. Figure 1(a) shows the arrangement of Li and M cations in the $Li_2Ti_2O_4$ spinel structure. The unit cell consists of a $2\times2\times2$ cubic supercell of the basic fcc primitive cell. Figures 1(b)–1(d) show the layered $LiNiO_2$ structure, the γ-$LiFeO_2$ structure, and the $LiMnO_2$ structure, respectively, in the same $2\times2\times2$ supercell. Each of the latter three structures can be described

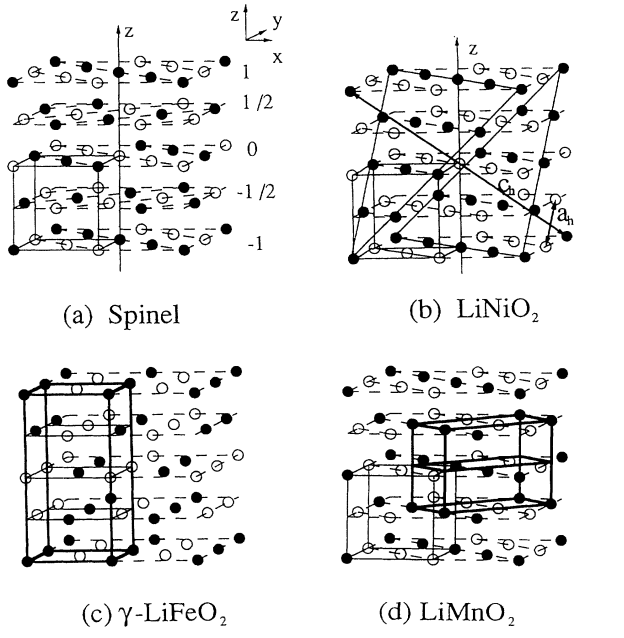

FIG. 1. The $2\times2\times2$ cubic supercell shows the cation positions only in (a) spinel structure (e.g., $Li_2Ti_2O_4$) (b) layered structure (e.g., $LiNiO_2$) (c) γ-$LiFeO_2$ structure and (d) $LiMnO_2$ structure. In (a) the conventional unit cell is equal to the size of the $2\times2\times2$ cell, while the conventional cells in (b), (c) and (d) are indicated with thick lines. The conventional fcc lattice is indicated with thin lines.

with a smaller unit cell, which we have indicated in the figures. When the structures are described with their conventional cells, the close structural relationship between the phases is not obvious. By showing the four structures on the same $2\times2\times2$ super cell we show the similarities between them. For example, $LiMnO_2$, $LiNiO_2$, and $Li_2Ti_2O_4$ are made up of [001] planes of identical structure with cation rows parallel to $\langle 110\rangle$. The structures only differ in the stacking sequence and rotation of the planes.

Here we show how a lattice-gas model with first- (J_1) and second- (J_2) neighbor interactions can be used to explain most of the observed structures of $LiMO_2$ compounds. The same model has already been applied to explain the cation ordering which occurs in $Li_xNi_{2-x}O_2$ (Ref. 8) as a function of composition x. Here, we fix the number of Li atoms and the number of transition-metal atoms to be each equal to half the number of oxygen atoms and investigate the phase diagram as a function of J_1, J_2, and T.

II. GROUND STATES

We start with a lattice-gas-model Hamiltonian,

$$H=\frac{1}{2}\sum_{r,r'} t_r t_{r'} J(\mathbf{r}-\mathbf{r}')+\mu\sum_r t_r \ , \tag{1}$$

where $\mathbf{r}$ is a position vector in the cation lattice, $t_{r'}$ has two states, $t_{r'}=1$, and $t_{r'}=0$, to designate that the site is filled by a transition metal or a lithium, respectively. $J(\mathbf{r}-\mathbf{r}')$ is the interaction potential between sites $\mathbf{r}$ and $\mathbf{r}'$ and μ is the chemical potential of the transition-metal atoms in the lattice. We use the convention that positive J corresponds to a repulsive interaction. Li-Li interactions are accounted for through the absence of M-M interactions.[8] J_1 and J_2 are denoted for the first- and the second-nearest-neighbor interactions, respectively. Figure 2 shows the 12 nearest neighbors and the 6 second-nearest neighbors.

The fcc lattice gas has been extensively studied with application to A-B alloys (see Ref. 9 for a review). We will draw heavily on that work here. The ground-state phase diagram of the fcc lattice gas with nearest-neighbor (NN) and next-nearest-neighbor (NNN) interactions has been calculated.[10] Figure 3 shows the ground-state phase diagram for the fcc lattice gas as a function of J_1 and J_2. Studies of the fcc lattice gas with repulsive (positive) J_1 and J_2, such that $J_2<J_1/2$, predict ground states with cations arranged as in γ-$LiFeO_2$.[10–12] For repulsive J_1 and J_2 such that $J_2>J_1/2$, the ground state[10–13] has cations segregated into alternate planes normal to the cubic $\langle 111\rangle$ directions as in CuPt. This is the cation arrangement observed in $LiNiO_2$. Furthermore, by analogy with their statements about CuPt, Richards and Cahn[12] imply without proof that the spinel atom arrangement found in LT-$LiCoO_2$ and in $Li_2Ti_2O_4$ is *energetically equivalent* to the layered arrangement. Clapp and Moss[10] did not mention the spinel phase in their work, but did identify phases with atoms arranged as in $LiNiO_2$ and γ-$LiFeO_2$. The ground states of the fcc lattice gas with first- and second-neighbor interactions listed in Ref. 9 include the

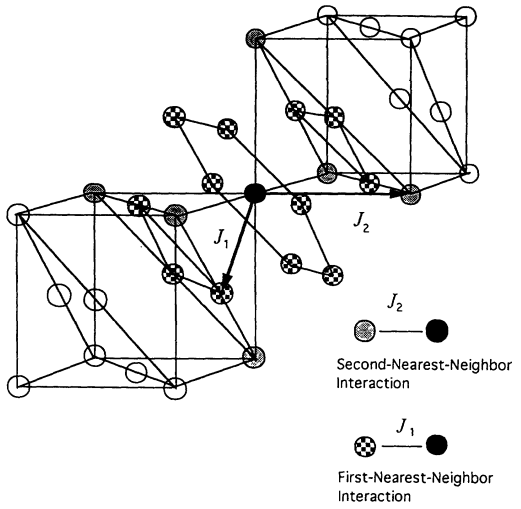

FIG. 2. The first-nearest-neighbor- and the second-nearest-neighbor interactions are shown for the black site in the cation lattice. The gray balls are the second-nearest-neighbor sites and the checkerboard balls are the first-nearest-neighbor sites.

degenerate layered and spinel structures. The authors of Ref. 9 state that the degeneracy is lifted if tetrahedron interactions are introduced. Gahn used Monte Carlo computer simulations to study the ground states of binary fcc structures with first- and second-nearest-neighbor interactions.[14] For $J_2/J_1>0.5$ and $J_1>0$, he reported that after cooling from the high-temperature disordered phase, only the layered structure appears. On the other hand, Phani and Lebowitz reported, based on privately communicated unpublished results,[15] that the spinel phase weakly dominates at low temperatures for the same

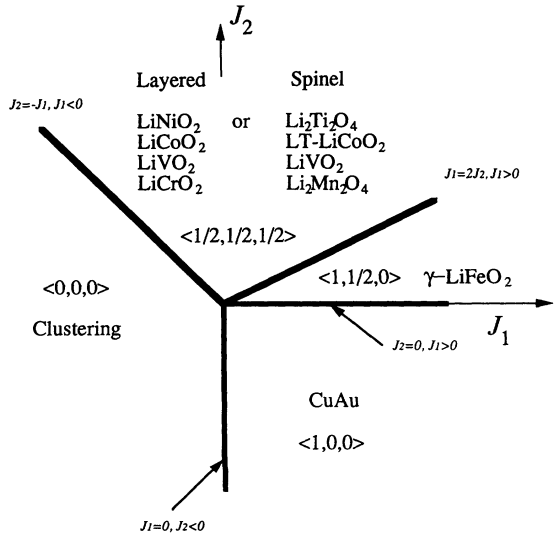

FIG. 3. The phase diagram of the fcc lattice predicted by mean-field theory as a function of J_1 and J_2. The positions of the layered, spinel, and γ-$LiFeO_2$ structures have been indicated as have the family of ordering wave vectors in each single-phase region.

set of interactions used by Gahn. Finel used the low-temperature series-expansion method to predict that the layered structure is the most stable for $J_1 > 0$, and the spinel is most stable for $J_1 < 0$.[16] Clearly, there is some confusion in the literature about the relative stability of these phases at finite temperature.

Monte Carlo methods are used here to investigate the structures for $x=1$ in $Li_xM_{2-x}O_2$ with first- and second-neighbor interactions. Our results show that the layered and spinel structures are degenerate not just at $T=0$; but also degenerate at $T>0$. The free energy and entropy of the two structures upon warming are the same (within statistical error) in the entire range of temperature $0 \le T \le T_C$ for various values of J_1 and J_2. The layered and spinel structures also appear with equal probabilities in cooling runs.

All of the ground states shown in Fig. 3 can be described in terms of Fourier modes or concentration waves, with various wave vectors. The layered $LiNiO_2$ structure corresponds to the $(\frac{1}{2}, \frac{1}{2}, \frac{1}{2})$ phase with a single wave vector and the spinel $Li_2Ti_2O_4$ phase corresponds to an equal mixture of the four $(\frac{1}{2}, \frac{1}{2}, \frac{1}{2})$ wave vectors, $\mathbf{q}_1=(\frac{1}{2},\frac{1}{2},\frac{1}{2})$, $\mathbf{q}_2=(\frac{1}{2}, -\frac{1}{2}, -\frac{1}{2})$, $\mathbf{q}_3=(-\frac{1}{2}, \frac{1}{2}, -\frac{1}{2})$, and $\mathbf{q}_4=(-\frac{1}{2}, -\frac{1}{2}, \frac{1}{2})$. In the region $J_1>0$ and $0<J_2<\frac{1}{2}J_1$, the wave vector $(\frac{1}{2}, 0, 1)$ corresponds to the structure of γ-$LiFeO_2$. For the lower right corner ($J_1>0$, $J_2<0$), wave vectors of the type (100) correspond to the structure of CuAu.

The literature cited above describes these ground states in the context of binary alloys with formula A_xB_{1-x} where $0 \le x \le 1$. If we write $LiMO_2$ as $2(A_xB_{1-x}O)$ with A=Li, B=transition metal, and $x=\frac{1}{2}$, the correspondence becomes clear. Table I provides a translation from the commonly used binary-alloy nomenclature and the corresponding $LiMO_2$ structures. This will be useful to readers interested in studying the binary-alloy literature.

By inspection of Figs. 1(a) and 1(b), the number of M-M contacts in each of the layered and spinel structures is equal to 6, which contributes $6J_1$ to the internal energy. Similarly, the number of second-neighbor (0) and third-neighbor (12) contacts is also identical. In fact, we will now prove that the number of M-M contacts at any distance in the two structures is the same! This is easily shown. Consider the atom at the origin (the center of the supercell) of Fig. 1(a). The spinel structure can be changed to the layered structure by rotating the (001) planes at $z=(n+\frac{1}{2})a$ by $\pi/2$ about the z axis. *No distances from any atom to the atom at the origin are changed by this rotation.* Since this choice of origin and axes is arbitrary, any point in each of two lattices has the same number and type of M-M, M-Li, and Li-Li contacts out to infinite distance. Thus the ground-state energies of the layered and spinel structures are the same, provided only pairwise interactions are included.

TABLE I. Structure types of AB alloys and $LiMO_2$ compounds.

Alloy Nomenclature	Binary alloy example	Lithium transition-metal oxides
$L1_1$	CuPt	$LiNiO_2$ (layered)
AB		$LiCoO_2$ (spinel)
A_2B_2		γ-$LiFeO_2$
$L1_0$	CuAu	

A model incorporating two-, three-, and four-body interactions has been used to explain more complex structures.[17] Clapp and Moss[10] determine the regions of ground-state stability for the fcc lattice gas with first-, second-, and third-neighbor interactions. Kanamori and Kakehashi report the ground states for arbitrary concentration with fourth-neighbor interactions.[18]

III. PHASE DIAGRAM AT FINITE TEMPERATURE

The J_1-J_2-T phase diagram for the fcc lattice-gas model is shown in Fig. 4. The center of the diagram corresponds to the high-temperature disordered phase with the rocksalt (NaCl) structure. No new ordered phases that do not exist at $T=0$ appear at finite temperature for $x=\frac{1}{2}$. For many values of $J_1>0$, the critical temperatures have been reported previously.[15,19,20]

We have also calculated critical temperatures for $J_1<0$ using the Monte Carlo method[21] on an $8\times8\times8$ fcc lattice. Critical temperatures were determined from the maximum in the fluctuations of the order parameter (i.e., the maximum in the ordering staggered susceptibility). The composition $x=\frac{1}{2}$ was maintained by fixing the transition-metal chemical potential,

$$\mu = -6J_1 - 3J_2 \ . \tag{2}$$

To compare our critical temperatures with those of much of the previous work, one must remember that lattice-gas-interaction constants (J's) will differ by a factor of 4, from those of an Ising model with a Hamiltonian of the form (1).

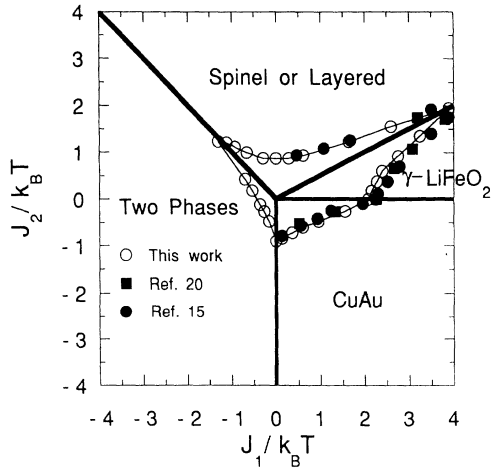

FIG. 4. The phase diagram calculated by Monte Carlo methods. The region inside the data points around the origin (0,0) is the high-temperature disordered phase. Outside the data points, where careful calculations were made, the ordered structures indicated are formed. The black circle and the black square data points are from Refs. 15 and 20, respectively.

As the layered and spinel structures are rather common for $LiMO_2$ materials, we feel it is important to study the relative stability of the structures at finite temperature. Just because the ground states are equal in energy by no means implies that the free energies or entropies are the same at finite temperature. If one structure has a higher density of low-lying excited states it will have a higher entropy at finite temperature, hence being stabilized *and* preferentially selected upon slow cooling. As mentioned above, some conflicting work on this question exists in the literature and, to our knowledge, no published Monte Carlo work exists for the case $J_1 < 0$. We hope to settle this question using both conventional Monte Carlo and recently introduced histogram Monte Carlo methods[22] by which the density of states and the entropy can be calculated directly.

As stated previously, and spinel structure can be converted to a layered structure by simply rotating every other layer [i.e., those labeled by half integers in Fig. 1(a)] by 90°, about the z direction. One can also extend this idea to excited states. Any low-lying excited state above the spinel ground state can be converted, by 90° rotation, to a corresponding low-lying excited state above a layered ground state. When $J_1=0$, the neighboring layers are uncoupled and there is no change in energy upon such rotation of any excited state. As a result, for every low-lying excited state above the spinel ground state there is a corresponding excited state above one of the layered ground states, with exactly the same energy. This one to one correspondence means that the density of low-lying excited states above the spinel and layered ground states is identical, and also that no thermal selection will occur upon slow cooling, when $J_1=0$. When $J_1\neq 0$, the neighboring layers become coupled and our simple proof no longer applies. Nevertheless, this rigorous result for $J_1=0$ provides an important test of the Monte Carlo methods described below, which we use to address the question of thermal selection when $J_1\neq 0$. Indeed, we find that for $J_1=0$, the Monte Carlo method predicts an identical (within statistical error) low-temperature entropy and density of low-lying excited states, upon warming from spinel and layered ground states. This gives us confidence in our Monte Carlo results for the case $J_1\neq 0$.

The transition-metal atom densities for the spinel and layered structures are described by the same set of four wave vectors, with Fourier amplitudes η_1, η_2, η_3, and η_4, respectively. Layered structures are described by any one of the four modes, whereas the spinel structure has equal contributions from all four modes. The root-mean squared Fourier amplitude,

$$\eta=(\eta_1^2+\eta_2^2+\eta_3^2+\eta_4^2)^{1/2} , \tag{3}$$

makes no distinction between the two phases. However, the order parameter,

$$\Delta=2(|\eta_1|+|\eta_2|+|\eta_3|+|\eta_4|)-3(\eta_1^2+\eta_2^2+\eta_3^2+\eta_4^2)^{1/2} , \tag{4}$$

is 1 for perfect spinel order and -1 for perfect layered order.

For interactions in the spinel and/or layered region of the phase diagram, slow annealing with the Monte Carlo method resulted in both the spinel and layered phases with 50% probabilities. This result was independent of the sign of J_1. This implies that the free energies of the spinel and layered phases are equal near T_c. Figure 5 shows the probability distribution of Δ, $[P(\Delta)]$, at temperatures near and below T_c. The area under the peaks in the distribution is $(50\pm 2)\%$ at any temperature. This shows that within statistical errors, the system is fluctuating between the two phases below T_c with equal probability. The number of Monte Carlo steps needed for a fluctuation between phases increases rapidly below T_c, making low-temperature studies of this problem with conventional Monte Carlo methods difficult.

The energy-probability distribution $P_\beta(E)$ at inverse temperature $\beta=1/kT$ can be calculated approximately by Monte Carlo methods using

$$P_\beta(E)=\frac{H_\beta(E)}{\sum_E H_\beta(E)} , \tag{5}$$

where the energy E is distributed over a finite number of discrete bins, and $H_\beta(E)$ is the number of Monte Carlo configurations generated with energy E during the simulation, i.e., $H_\beta(E)$ is an energy histogram obtained from a simulation at inverse temperature β. If $P_\beta(E)$ is known

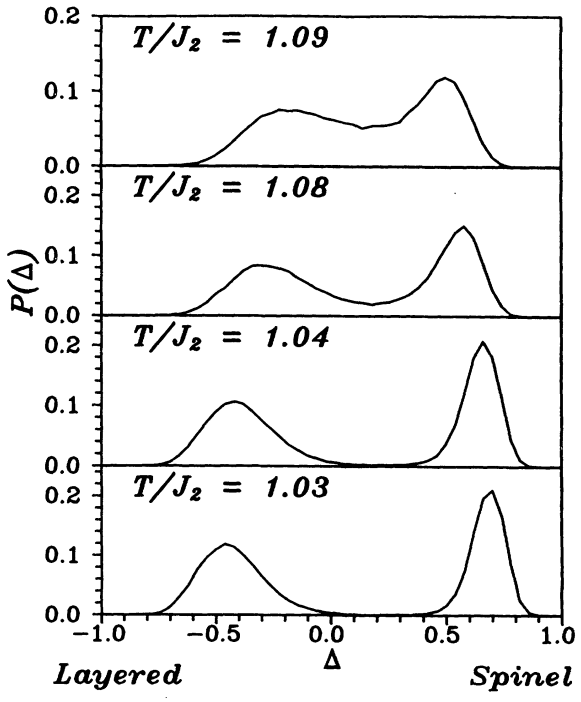

FIG. 5. The probability $P(\Delta)$ of finding a particular value of Δ. The layered and spinel phases appear with equal probability for various temperatures below T_c. The calculation is for an $8\times 8\times 8$ lattice using $J_1=0$. 1.0×10^6 Monte Carlo steps per site were used to generate the probability distribution. Similar results are obtained for various values of J_1, provided one stays in the region of stability of the spinel and layered phases.

then the density of states can also be calculated from

$$P_\beta(E)=\frac{W(E)e^{-\beta E}}{\sum_E W(E)e^{-\beta E}}=\frac{W(E)e^{-\beta E}}{Z_\beta}\ , \tag{6}$$

where $W(E)$ is density of states and Z_β is the partition function. In practice, $H_\beta(E)$ will contain statistical noise due to the finite duration of the simulation. Assuming Poisson statistics, the statistical error in $H_\beta(E)$ is simply $H_\beta(E)^{1/2}$. Since $P_\beta(E)$ is strongly peaked near $\langle E\rangle_\beta$, the counting statistics in the wings of the distribution will be very poor. This problem can be overcome by combining histograms from simulations at many different temperatures selected in such a way that all energy bins receive sufficient sampling. The histograms are then combined in an optimal manner, described in Ref. 22, resulting in an estimate for the density of states $W(E)$ or the entropy S_β.

Here we use an $8\times8\times8$ fcc lattice. The spinel and the layered structures are introduced in the lattice at very low temperature (0.1 T_c). The system is then gradually warmed up to a very high temperature (10 000 T_c). The temperatures are properly chosen to ensure that all energy bins receive sufficient sampling. The relative uncertainty of $W(E)$ is proportional to $1/\sqrt{H_i(E)}$. For each temperature, 5×10^4 Monte Carlo steps are summed, giving 2×10^6 configurations over a total of 40 temperature points.

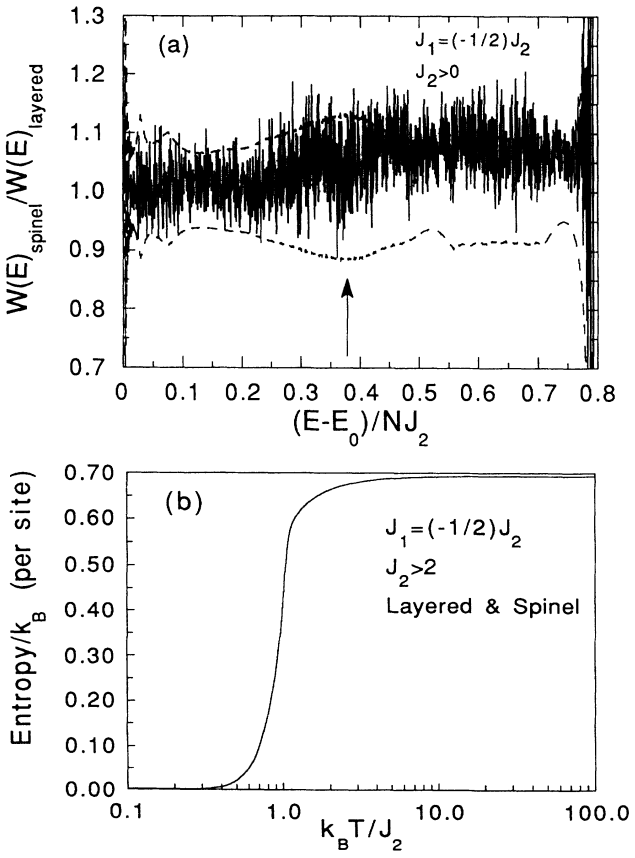

FIG. 6. (a) Ratio of density of states $W(E)$ for spinel and layered structures are shown as calculated using Monte Carlo methods. The dashed lines show the positive and negative ($\pm\sigma$) error estimations. E_0 is the ground-state energy. The arrow indicates the value of $\langle E-E_0\rangle_{T=T_c}/NJ_2=0.376$. (b) Entropy per site S is shown vs k_BT/J_2 for layered and spinel structures. The difference in S/N for the two structures is less than $5\times10^{-5}\,k_B$.

The spinel and layered ground states are each eightfold degenerate. Hence the total degeneracy of the ground state is 16, and the entropy equals ln 16 at $T=0$. When T is infinite, the entropy of the system is $N\ln2$ (N is the total number of the sites). Therefore, the entropy of the layered phase and the spinel phase equal each other at $T=0$, and $T=\infty$, without dependence on J_1 and J_2. The difference in entropy of spinel and layered structures at low temperatures is calculated by warming up from their ground states, and by equalizing the entropy at $T=0$ for the two structures. This can be thought of as a low-temperature expansion calculated by Monte Carlo methods.

The Monte Carlo method is used to calculate $W(E)$ and the entropy of the spinel and layered structures for $J_1=0$, $J_1<0$, and $J_1>0$, respectively. Figure 6(a) shows the results of the ratio of $W(E)$ for the two structures after warming for $J_1=-(\frac{1}{2})J_2<0$. The results are similar for cases of $J_1=0$ and $J_1>0$. The statistical error estimation is shown at the same time with two dashed lines. E_0 is the ground-state energy. For $(E-E_0)/NJ_2$ near zero, the error estimation is quite large since some energy bins were sampled very infrequently. For $(E-E_0)/NJ_2$ near 0.8, which corresponds to very high-temperature excitations, the error estimation is also large because these bins are at energies greater than $\langle E\rangle_{T=\infty}$ and are, therefore, infrequently sampled. The arrow indicates the average energy at the critical temperature $\langle E\rangle_{T_c}$. Clearly, the difference between $W(E)_{\text{spinel}}$ and $W(E)_{\text{layer}}$ for $E<\langle E\rangle_{T_c}$ is within the estimated error. That means there is no difference in the density of excited states for the layered and spinel structures within statistical error. Figure 6(b) shows the entropy per site S/N vs temperature for the layered and spinel structures. For the entire range of the temperature, the difference of S/N for two structures is on the order of $5.0\times10^{-5}\,k_B$, which is too small to see in Fig. 6(b). We conclude that the spinel and layered structures have identical free energy and entropy in the region of where $-J_2<J_1<2J_2$ and $J_2>0$.

IV. SUMMARY AND CONCLUSIONS

The structures of lithium transition-metal oxides $LiMO_2$ are related to binary alloys, and can be explained with the lattice-gas model. The spinel and layered structures, which are common in $LiMO_2$ compounds are proved to have energetically identical ground states, for arbitrary pairwise interactions out to any distance. Furthermore, we prove that the spinel and layered structures have identical free energies and entropies for $J_1=0$. Using Monte Carlo methods, we extend the conclusion to the region of $-J_2<J_1<2J_2$ and $J_2>0$ where the spinel and layered structures also have identical free energy and

entropy (within statistical error) in the entire range of temperature.

Distortions of the fcc lattice occur in $LiNiO_2$ $LiCrO_2$, layered $LiCoO_2$, and layered $LiVO_2$. The distortion breaks the degeneracy of the spinel and layered phases. This is because J_1 takes on two values, one for the six atoms in the same (111) plane (normal to the Li and Ni layers) and one for the six atoms in the neighboring (111) planes (see Fig. 1). Therefore, real materials may be able to lower their energy by a distortion; $LiNiO_2$, $LiCrO_2$, layered $LiCoO_2$, and layered $LiVO_2$ are examples of this, where the distortion is only one or two percent. In $LiMnO_2$, there is a large distortion [the $2\times2\times2$ supercell in Fig. 1(d) is stretched by 14% in the vertical direction[23]], presumably caused by the Jahn-Teller effect. The anisotropies in the J's definitely need to be accounted for to explain this structure.

Recent studies of $Li_xNi_{1-x}O$ with $0.1<x<0.5$ (Ref. 8) showed that the same lattice-gas model could fit the order-disorder transition from the disordered rocksalt phase to the layered phase, but only if $J_2>2|J_1|$. It is a challenge to all materials theorists to understand why NNN interactions are stronger than NN atom-atom interactions, in $LiMO_2$ compounds with layered and spinel structures.

Scientists studying lithium transition-metal oxides must beware. Phase transitions between spinel and layered phases may occur as a function of lithium concentration in $Li_{1-x}M_xO$ or, perhaps, as a function of applied pressure. For example, the spinel $LiVO_2$ phase can only be prepared at high pressure. Since the unit-cell volume of layered $LiCoO_2$ is slightly larger than that of spinel $LiCoO_2$, it is likely that a transition from the layered to the spinel phases will occur with applied pressure. Pressure-dependent studies of CuPt may also induce such a transition.

[1]T. Nagaura and K. Tozawa, Prog. Batt. Sol. Cells **9**, 209 (1990).
[2]J. R. Dahn, U. Von Sacken, M. W. Juzkow, and H. J. Al-Janaby, J. Electrochem. Soc. **138**, 2207 (1991).
[3]R. B. Goldner, F. O. Arntz, G. Berera, T. E. Haas, G. Wei, K. K. Wong, and P. C. Yu, Solid State Ionics, **53-56**, 617 (1992).
[4]C. Delmas, Mat. Sci. Eng. B **3**, 97 (1989).
[5]T. A. Hewston and B. L. Chamberland, J. Phys. Chem. Solids **48**, 97 (1987).
[6]E. Rossen, J. Reimers, and J. R. Dahn, Solid State Ionics **62**, 53 (1993).
[7]R. J. Gummow, D. C. Liles, and M. M. Thackeray, Mater. Res. Bull. **28**, 235 (1993).
[8]W. Li, J. N. Reimers, and J. R. Dahn, Phys. Rev. B **46**, 3236 (1992).
[9]F. Ducastelle, *Order and Phase Stability In Alloys* (North-Holland, Amsterdam, 1991).
[10]Phillip C. Clapp and S. C. Moss, Phys. Rev. **171**, 754 (1968).
[11]J. M. Sanchez and D. de Fontaine, Phys. Rev. B **21**, 216 (1980).
[12]M. S. Richards and J. M. Cahn, Acta Metall. **19**, 1263 (1971).
[13]S. M. Allen and J. W. Cahn, Acta Metall. **20**, 423 (1972).
[14]Ulrich Gahn, J. Phys. Chem. Solids **43**, 977 (1982).
[15]M. K. Phani and Joel L. Lebowtiz, Phys. Rev. B **21**, 4027 (1980).
[16]A. Finel, Ph.D. thesis, University of Paris, 1987.
[17]Daniel F. Styer, Mohan K. Phani, and Joel L. Lebowitz, Phys. Rev. B **34**, 3361 (1986).
[18]J. Kanamori and Y. Kakehashi, J. Phys. (Paris) Colloq. **38**, C7-274 (1977).
[19]K. Binder, Phys. Rev. Lett. **45**, 811 (1980).
[20]J. M. Sanchez and D. de Fontaine, Phys. Rev. B **25**, 1759 (1982); T. Mohri, J. M. Sanchez, and D. de Fontaine, Acta Metall. **33**, 1171 (1985).
[21]K. Binder, *Monte Carlo Methods in Statistical Physics* (Springer-Verlag, Berlin, 1986).
[22]Alan M. Ferrenberg and Robert H. Swendsen, Comput. Phys. **3**, 101 (1989).
[23]R. Hoppe, G. Brachtel, and M. Jansen, Z. Anorg. Allg. Chem. **417**, 1 (1975).

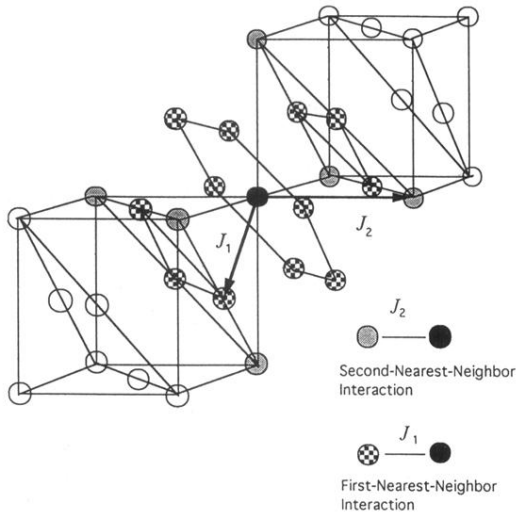

FIG. 2. The first-nearest-neighbor- and the second-nearest-neighbor interactions are shown for the black site in the cation lattice. The gray balls are the second-nearest-neighbor sites and the checkerboard balls are the first-nearest-neighbor sites.